Polymer 51 (2010) 1485–1493

Contents lists available at ScienceDirect

Polymer

journal homepage: www.elsevier.com/locate/polymer

Impact of nanosilicates on poly(vinylidene fluoride) crystal polymorphism: Part 1. Melt-crystallization at high supercooling

B. Seyhan Ince-Gunduz [a], Robert Alpern [b], Debeshu Amare [c], Jennifer Crawford [a], Breanna Dolan [d], Stacey Jones [c], Ryan Kobylarz [c], Matthew Reveley [a], Peggy Cebe [a,*]

[a] Tufts University, Department of Physics and Astronomy, Medford, MA 02155, USA
[b] Rochester Institute of Technology, Mechanical Engineering Department, Rochester, NY 14623, USA
[c] Gallaudet University, Department of Chemistry and Physics, Washington, DC 20002, USA
[d] Rochester Institute of Technology, Department of Biotechnology, Rochester, NY 14623, USA

ARTICLE INFO

Article history:
Received 13 August 2009
Received in revised form
4 January 2010
Accepted 7 January 2010
Available online 28 January 2010

Keywords:
Nanocomposites
Poly(vinylidene fluoride)
Phase identification

ABSTRACT

Polymorphism of poly(vinylidene fluoride), PVDF, in the presence of Lucentite STN organically modified silicate (OMS) is investigated for PVDF nanocomposites melt-crystallized at high supercooling temperatures where neat PVDF crystallizes exclusively in the alpha crystalline phase. Nanocomposites were prepared from solution with 0–1.0 wt% OMS composition. Here we observed that clay addition promotes gamma phase formation in nanocomposites melt-crystallized at high supercooling (i.e., at low crystallization temperature), whereas previously we showed that even small amount of nanosilicates resulted in beta phase formation in cold-crystallized PVDF nanocomposites [1].

Wide-angle X-ray scattering (WAXS), Fourier transform infrared spectroscopy (FTIR) and differential scanning calorimetry (DSC) studies showed that α- and γ-phases co-existed in nanocomposites containing up to 0.1 wt% OMS, and the amount of α-crystals substantially diminished for higher OMS content. Formation of γ-crystal phase was confirmed with morphologic observation of spherulites of low-birefringence using polarizing optical and atomic force microscopies, and their crystalline structures were verified by FTIR and Raman microscopic spectroscopy. We also address in this work the ambiguities in assessing PVDF crystallographic phases, and correct the phase identification errors which have persisted up to this point in the literature based on melting point confusion. The crystal phase identification for PVDF nanocomposites is discussed and clarified, based on X-ray scattering, vibrational spectra, and thermal analysis. For reference, we provide a vibrational band list, indicating the close, or overlapping bands, of the three phases of PVDF: α, β and γ.

1. Introduction

In a previous work we studied addition of organically modified silicates (OMS) to PVDF in the range from 0.01 to 20 wt% OMS in their cold-crystallized state [1]. The formation of a second phase, beta phase, was observed along with alpha phase as OMS was added to PVDF at even a small amount, 0.01% OMS by weight. We found that beta phase started being dominant once the OMS content exceeded 0.025%.

In our work, we focus on melt-crystallization of nanocomposites of poly(vinylidene fluoride), PVDF, based on two thermal schemes: (1) at "high" supercooling temperatures (i.e., $T < 155\,^{\circ}C$) [2], reported herein; and, (2) at "low" supercooling (i.e., $T > 155\,^{\circ}C$) [2] which will be the subject of a future report. Upon melt-crystallization, depending on its supercooling range, neat PVDF produces either alpha phase, or gamma along with alpha phase. For "high" supercooling, at temperatures lower than about 150–155 °C, only alpha phase is observed [3–5]; for "low" supercooling, at temperatures higher than 155 °C, gamma and alpha phase mixtures are observed [6–8]. However since growth rates of gamma crystals are very low compared to alpha crystals, for dominant or complete gamma crystal formation to occur a sufficiently long crystallization time at high temperature is needed [9–11]. Therefore no report exists in the literature showing 100% gamma-PVDF occurring from melt-crystallization. Here, the terms "high" and "low" supercooling are used according to the crystal phases that homopolymer PVDF exhibits at those melt-crystallization temperatures.

To investigate the effect of clay addition on phase behaviors of nanocomposites at lower melt-crystallization temperatures (i.e. high supercooling temperatures) we chose a temperature

* Corresponding author. Tel.: +1 617 627 3365; fax: +1 617 627 3744.
E-mail address: peggy.cebe@tufts.edu (P. Cebe).

0032-3861/$ – see front matter © 2010 Elsevier Ltd. All rights reserved.
doi:10.1016/j.polymer.2010.01.011

comparable to our previously reported cold-crystallization work [1]. For morphological observation purposes an optimum temperature had to be chosen so that spherulitic structure could be examined dynamically as well. Hence, the melt-crystallization temperature for the "high" supercooling protocol was established as 150 °C at which temperature neat PVDF shows exclusively alpha phase crystals [3–5].

There are many literature reports on studies of nanocomposites of PVDF with different fillers [12–16]. Among them several authors study melt-crystallization of PVDF nanocomposites. Asai et al. explored crystallization kinetics and structure of nanocomposites with layered titanate (HTO) in the crystallization temperature range of 110–150 °C [17]. They found that PVDF/HTO at lower T_c (110–135 °C) exhibited a majority of α-phase crystals co-existing with β and γ, while for a higher T_c (140–150 °C), mainly γ-crystals were observed together with α and β crystal forms. They also compared HTO with synthetic fluorine hectorite and montmorillonite (MMT) nanofillers and showed the majority of crystals are γ-crystals for the high T_c range, independent of organoclay. However for lower crystallization temperatures, surface charge densities of organoclays play a role in formation of different polymorphs. Dillon et al. [18] studied the impact of different preparation methods of PVDF/Cloisite nanocomposites on their morphology; as a part of their work it was shown that Cloisite 15A acted as nucleation agent when nanocomposites are crystallized at 152 °C from the melt for 6 h. At this thermal treatment they observed very tiny spherulites having no dimensions measurable by optical means [18]. Song et al. used SiO_2 as the nanofiller with different attached chemical groups. They applied non-isothermal crystallization to nanocomposites and observed that the type of nanosilica affects the resulting phase [19]. Patro et al. showed there was a decrease in spherulite size for nanocomposites of MMT clay with PVDF, when the effects of unmodified clays and clays with different modifiers on PVDF crystals [20] were compared.

In the literature on PVDF nanocomposites, after melt-crystallization or using other crystallization methods, it is shown that nanofillers induce a new phase, either beta or gamma (mostly beta), or the nanocomposites have mixtures of alpha, beta, or gamma crystals. The fact that gamma and beta type crystals have very similar infrared spectra and similar WAXS diffractograms, as well as literature confusion on the melting point of beta (see Results and discussion), introduces an ambiguity in the determination of the crystal phases. Ramasundaram et al [21]. pointed out some of these issues and compared as-cast, quenched, and non-isothermally slowly cooled nanocomposites. They suggested an ion–dipole interaction between clay platelets and PVDF chains favors beta formation when samples were melt-quenched.

In our work, we focus on isothermal melt-crystallization at a high supercooling temperature. Nanocomposites of poly(-vinylidene fluoride) with Lucentite STN™ organically modified silicate (OMS) are studied in the range from 0 to 1% of OMS by weight. The questions addressed in this work are: 1. Does addition of OMS promote a different crystal phase other than alpha phase under isothermal melt-crystallization at high supercooling? 2. What impact on morphology is brought when nanocomposites are crystallized from the melt at 150 °C, a temperature that forms only brightly birefringent alpha phase spherulites with concentric banding in neat PVDF? and, 3. What effects are observed compared to cold-crystallized nanocomposites which favored beta phase?

2. Experimental section

2.1. Sample preparation

Kynar based PVDF material is obtained from Elf Atochem as grade 740, in pellet form. Lucentite STN™, was obtained from Zen-Noh Unico, Americas (currently CBC Chemical Company, Japan), as fine powder [22]. Lucentite is an organically modified layered silicate prepared by the supplier by ion-exchanging the Na ions in a synthetic smectite clay (Lucentite SWN, with a cation exchange capacity of approximately 0.65 meq/g) for tri octyl methyl ammonium cations [22].

The films of PVDF-OMS nanocomposites were obtained from the mixture of their separate solutions in dimethylacetamide (DMAc) in desired compositions. Solutions were stirred at room temperature for 1–2 days and subsequently mixed with different percentages of OMS, ranging from 0.01 to 1.0% OMS by weight. Aliquots were reserved for morphological studies. The mixtures were stirred for several hours at room temperature, and after ultra-sonicating for 10 min they were poured into Petri dishes to dry. Evaporation of DMAc occurred in about three days; sometimes gentle heating to 70–80 °C was used to assist DMAc removal. Finally, the dried films were kept in a vacuum oven for a day or more at room temperature. To get a smoother film, they were compression molded at 200 °C for 2 min, and then quenched into cold water. Melt-crystallized bulk films were obtained by isothermal crystallization of the quenched films. Films were first heated to 200 °C in a Mettler hot stage to remove prior thermal history, and then cooled at 10 °C/min to 150 °C where they were held for 1 h. For morphological studies, a droplet of solution (from 15-min ultra-sonicated aliquots) was placed on a glass cover slip and the same melt-crystallization treatment was repeated in the Linkam THMS optical microscope hot stage.

2.2. Analysis methods

Wide-angle X-ray scattering (WAXS) studies were done using a conventional sealed tube X-ray source having $\lambda = 0.1542$ nm. A Phillips PW1830 X-ray generator, operated at 40 kV and 45 ma, and optically encoded diffractometer, were used to investigate the range of scattering angles from $2\theta = 2$–30 degrees (for θ the half-scattering angle). Films were examined in $\theta/2\theta$ reflection mode, using a step scan interval of 0.015 degrees with 2.4 s/step. D-spacings were calibrated using silicon powder reference standard placed on the film surface. The PVDF crystal peaks and amorphous halo were modeled using Gaussian wavefunctions as described previously [1].

Real-time WAXS was performed at the Brookhaven National Laboratory, National Synchrotron Light Source, at beamline X27C. The wavelength was 0.1371 nm, and d-spacing was calibrated using sodalite and silicon. The sample was encapsulated using high temperature Kapton™ tape, and heated inside a Mettler FP90 hot stage. Intensity was accumulated every 10 s during heating at 10 °C/min from 150 to 200 °C after the sample crystallized at 150 °C from the melt. The intensity was corrected for changes in the incident beam intensity, sample absorption, and Kapton™ background.

For morphology studies a Nikon Eclipse E600 Polarizing Optical Microscope (POM) with CCD camera was used with the Linkam THMS 600 hot stage unit. Melt-crystallized droplets of PVDF/OMS on glass cover slips were heated to 200 °C at 10 °C/min to observe melting, and subsequently cooled at 10 °C/min and crystallized isothermally at 150 °C for one hour. Spherulitic growth and impingement time were monitored under crossed polarizers using a camera mounted on the microscope. Static and real-time polarized images of the samples were obtained for different compositions of OMS. The linear growth rate was determined from the slope of spherulite diameter plotted against time.

Infrared studies on bulk films were performed using a Bruker Equinox 55 Fourier Transform infrared spectrometer and a Jasco FTIR equipped with an attenuated total reflectance cell. A diamond

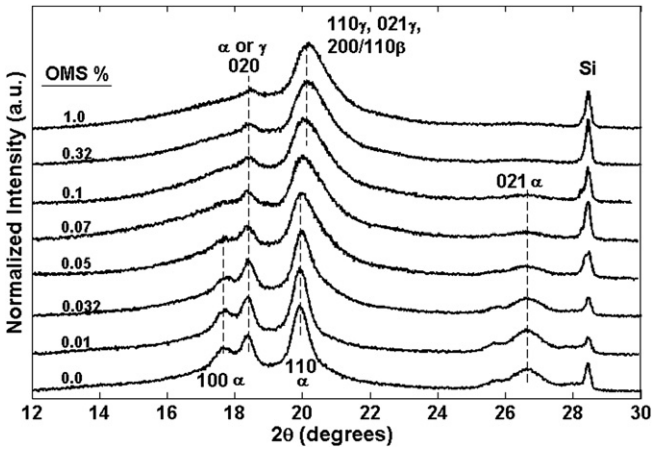

Fig. 1. Room temperature X-ray intensity ($\lambda = 0.1542$ nm) of PVDF/OMS nanocomposites at the indicated compositions. The curves are displaced vertically for clarity. Miller indices are marked for several of the predominant peaks.

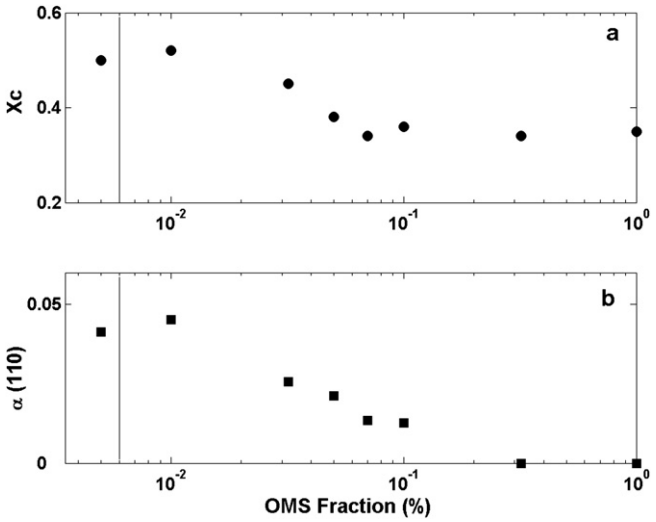

Fig. 3. (a) Crystallinity index from WAXS area ratio, A_C/A_T; and (b) (100) alpha peak crystal fraction from WAXS area ratio, A_{110}/A_T, of PVDF/OMS nanocomposites at room temperature. The data at the left side of the figure, separated by a straight line, are from PVDF homopolymer (0% OMS) and the *x*-axis scaling does not apply to these points, which are included for comparison only.

ATR crystal was used to examine low frequencies in the range 400–500 cm^{-1}. The FTIR spectra of different spherulites were obtained by using the IR microscopy unit in transmission mode. This unit allows the image to be masked so that different morphological features could be examined independently. The resolution was either 4 cm^{-1} or 2 cm^{-1} for FTIR and 32 or 256 scans were co-added to improve the signal to noise. Spherulites with different appearance and birefringence were also investigated with Raman spectroscopy using an HJY confocal Raman microscope.

Differential scanning calorimetry (DSC) was performed on a TA Instruments 2920 Modulated DSC at a heating rate of 10 °C/min. Heat flow and temperature were calibrated using indium. Endotherms are presented with downward deflection. The degree of crystallinity of PVDF was determined from the endotherm area using 104.6 J/g as the heat of fusion of 100% crystalline PVDF [23].

3. Results and discussion

3.1. Wide-angle X-ray scattering (WAXS)

Room temperature composite WAXS scans are shown in Fig. 1. For homopolymer PVDF (bottom curve) alpha phase reflections with d-spacings $d_{100}(\alpha) = 0.49$ nm, $d_{020}(\alpha) = 0.48$ nm, $d_{110}(\alpha) = 0.44$ nm and $d_{021}(\alpha) = 0.33$ nm, are observed clearly at the 2θ angles 17.66, 18.3, 19.9, and 26.7 degrees, respectively [24,25]. Two other reflections at higher angles appearing as shoulders on (021) peak, at 25.8 and 28.1 degrees, correspond to $d_{120}(\alpha) = 0.34$ nm and $d_{111}(\alpha) = 0.32$ nm. Gamma crystal planes are known to have very similar WAXS reflections to the ones of beta and alpha phase crystals [26]. The peak on the lowest angle side with Miller indices (100) is the only peak among the major alpha characteristic peaks that does not have any possibility of overlapping reflections with gamma phase. D-spacings of gamma reflections at $d_{020}(\gamma) = 0.480$, $d_{110}(\gamma) = 0.442$ and $d_{022}(\gamma) = 0.333$ nm overlap with (020), (110) and (021) alpha crystal planes, respectively. These overlapping reflections do not allow us to detect if there exists any small amount of gamma phase in neat PVDF solely from WAXS data. However, in FTIR data (shown below) we did not see any indication of gamma crystals for homopolymer PVDF.

As clay is added to PVDF, the (100) peak of alpha phase at $2\theta = 17.66°$ starts to diminish, and vanishes for nanocomposites with OMS contents of 0.32% and 1.0%. Similarly, the peaks on the higher angle side show a decrease with introduction of OMS leaving only a slight reflection at the highest PVDF/OMS compositions. In samples containing the two largest amounts of OMS, the (100) peak of alpha is not observed which indicates that the peak at $2\theta = 18.3°$ belongs to (020) gamma reflection for those compositions. The major peak at $2\theta = 19.90°$ broadens and shifts to higher angle, $2\theta = 20.20°$ upon adding of OMS, as a result of new crystal phase introduction. This newly emerging peak might be attributed to beta phase characteristic reflection 200/110 with a d-spacing 0.427 nm, but there is also a gamma reflection $d_{021}(\gamma) = 0.431$ nm in the same

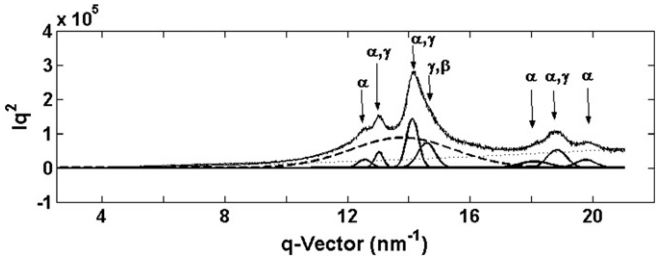

Fig. 2. Fitting of WAXS peaks of PVDF containing 0.05% OMS. Data curve shows WAXS intensity, $I(q)q^2$ vs. q, after silicon, background, and Lorentz-corrections were applied. Heavy solid lines represent individual Gaussian fitted peaks, which are plotted after subtraction of a baseline shown in dotted line. Heavy dashed line is the Gaussian fitted peak for the amorphous halo. The thin dotted line is the quadratic baseline. The thin solid line passing through the data curve is the summation of the baseline and fitted peaks. Possible phases corresponding to each peak are indicated on the figure.

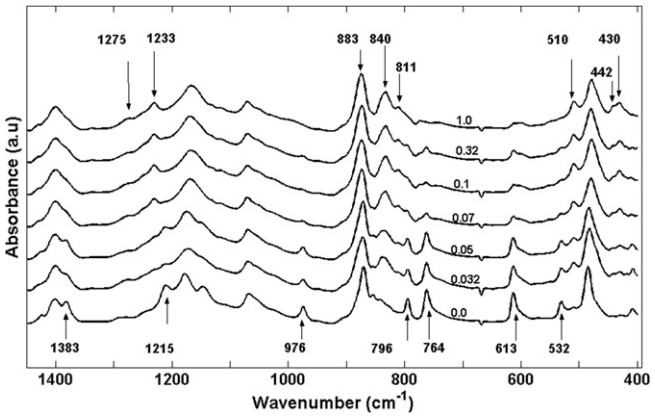

Fig. 4. FTIR absorbance spectra of PVDF/OMS melt-crystallization at 150 °C for 1 h. The curves are displaced vertically for clarity. Several prominent vibrational band positions are noted from the literature [29–31]. Bands across the bottom are related to alpha phase; bands across the top are related to beta or gamma phase.

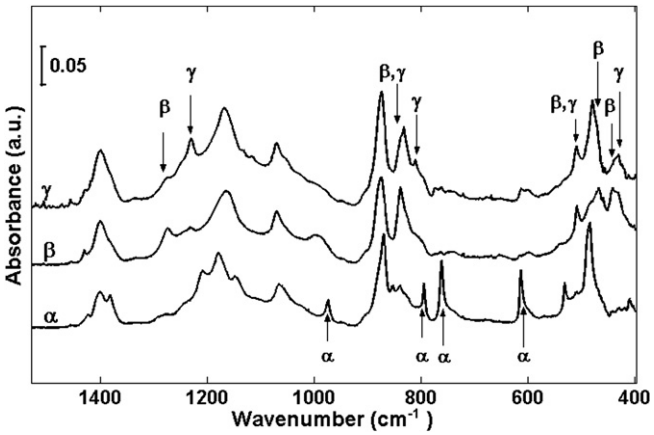

Fig. 5. FTIR spectra of PVDF nanocomposites which are exemplars representing three different PVDF phases. Each sample includes a dominant phase of α, β or γ as indicated. α-dominant sample is quenched neat PVDF; β-dominant sample is prepared by annealing quenched PVDF with 4% OMS at 145 °C; and γ-dominant sample is a 150 °C melt-crystallized PVDF/OMS nanocomposite with 1.0% OMS.

position [26,27]. To the readers, please note, we did not observe any notable reflection of the unique gamma peak, (111) with a d-spacing 0.39 nm at $2\theta = 22.3°$, except a broad shoulder for nanocomposites with 0.32% and 1.0% OMS [26]. However this is a weak-strength peak and is only slightly noticeable, even for samples crystallized at low supercooling degrees for a long time, which are deemed to have large γ content [2].

We did not observe any peaks for $2\theta < 10°$, i.e., there is no reflection from OMS silicate layers (data are not shown here for the sake of brevity), indicating Lucentite OMS layers are not intercalated but could be exfoliated in these nanocomposite samples. It also cannot be ruled out that such a small concentration of OMS in the polymer matrix could result in non-observation of gallery space reflections. However in cold-crystallized samples [1], the gallery spacing for Lucentite™ OMS was observed in compositions at or greater than 0.1 wt% OMS.

The crystallinity index is calculated by deconvolution of WAXS peaks using Gaussian fitting (as described previously [1,28]). An example of fitting is exhibited in Fig. 2 for 0.05% OMS, which shows the Lorentz-corrected intensity vs. scattering vector, q ($q = 4\pi\sin\theta/\lambda$ for θ the half-scattering angle). Possible crystal phases corresponding to individual peaks are marked on the figure. WAXS data alone are not sufficient to determine whether the samples containing Lucentite STN are in gamma phase only, or contain a mixture of beta and gamma.

Table 1
IR absorption bands[#] of major crystal phases of PVDF, for wavenumber range 400–1500 cm^{-1}.

α-PVDF	β-PVDF	γ-PVDF
488	444[a]	430[b]
530	467[a]	440
761	510*	510*
796	840*	775
875	884*	811[b]
976	1175	834, 838*
1210	1275[a]	883*
1383		1175
		1234[b]

Band assignments have been made by reference to the literature [29–31].
* Beta and gamma bands having very close vibrational frequencies.
[a] Characteristic beta phase absorption bands having no overlap with other absorptions.
[b] Characteristic gamma phase absorption bands having no overlap with other absorptions.

Crystallinity index, χ_c, as shown in Fig. 3a, decreases as OMS content increases, mainly for OMS content from 0.01 to 0.1%. Neat PVDF has $\chi_c = 0.50$ while $\chi_c = 0.36$ for the nanocomposites with 1.0% OMS. Due to the overlap of different crystal phase peaks, we were not able to calculate the amount of alpha, beta, or gamma phase crystals separately. The fraction of the only non-overlapping peak of alpha, (100), given in Fig. 3b, was found to decrease for OMS content up to 0.1%, and is zero for higher OMS content. Also, for the highest two compositions, 0.32% and 1.0%, we were able to fit a beta peak at around $2\theta = 20.75°$. But, for lower compositions, beta peak existence cannot be resolved indicating either it does not exist, or it is too small to detect, and cannot be resolved from the gamma peak overlapping it at that position. Although one cannot determine the phases quantitatively using WAXS, it can be concluded that the gamma phase is more favorable for melt-crystallized PVDF/OMS samples when OMS content increases in the range 0–1%.

These results show a clear difference when compared to our prior work on cold-crystallized nanocomposites, in which only beta phase crystals exist once OMS content exceeds 0.5 wt% [1]. The impact of melt-crystallization at 150 °C is to form the gamma phase crystals, with possibly also some small amount of beta crystals, when organically modified silicates are added to PVDF. This was explained by Ramasundaram et al. [21]. using an ion–dipole interaction of PVDF with OMS in the molten state. The interaction between the partially positive CH_2 dipoles of PVDF and the negatively charged clay nanolayers causes the polymer chain to become aligned on the clay platelet surface, favoring beta or gamma crystal nucleation [21]. When there is sufficient time during cooling from the melt, gamma nucleation and growth are preferred over beta, due to the more flexible chain conformation of gamma crystals, TTTGTTTG′. Consequently, isothermal melt-crystallization favors growth of gamma crystals.

3.2. Vibrational spectra

Fig. 4 shows FTIR spectra of melt-crystallized PVDF/OMS nanocomposites from 400 to 1500 cm^{-1}. The absorption band assignment has been made by reference to the literature [29–31]. No absorption bands of DMAc were seen, indicating complete removal of DMAc. The bands at 532, 764, 796, 976, 1215 and 1385 cm^{-1} are assigned to characteristic peaks of alpha phase and are clearly observed in neat PVDF. In melt-crystallized nanocomposites, at 0.07 wt% OMS and greater, gamma phase dominates, with

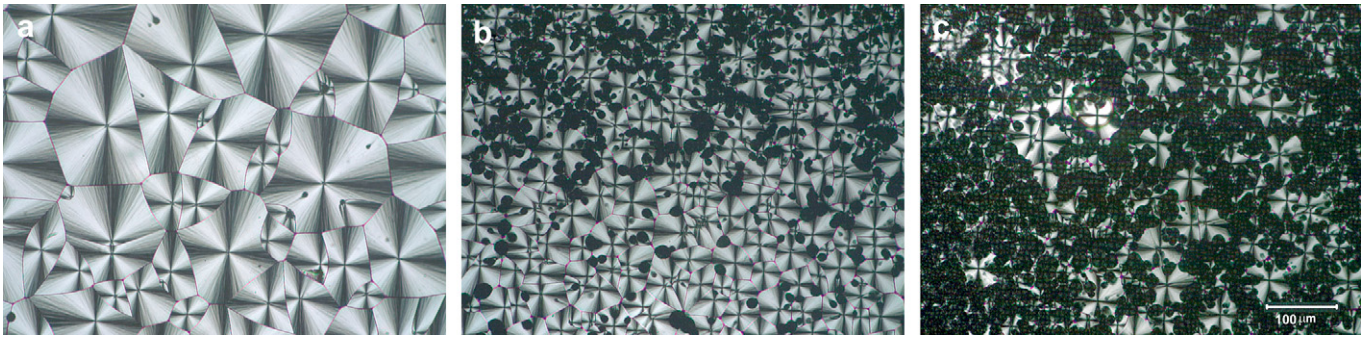

Fig. 6. (a–c) Polarizing optical microscopy images (A ⊥ P) taken at room temperature of PVDF and PVDF/OMS nanocomposite samples melt-crystallized at 150 °C for 1 h. (a) Neat PVDF; (b) 0.032% OMS; (c) 0.07% OMS. The scale bar represents 100 μm, and is the same for all parts of the figure.

characteristic peaks at frequencies 430, 510, 811, 840, 884, and 1233 cm^{-1}. Due to the existence of TTT in the chain conformation in both gamma and beta phases of PVDF [32], most of the absorption bands for these two phases appear at the same, or very similar, frequencies in the FTIR spectra. Accordingly, the bands at 510, 840, and 883 cm^{-1} are also characteristic of beta phase absorption. In addition, the beta form of PVDF has characteristic bands at 444, 467 and 1275 cm^{-1}. We use 811 and 1233 cm^{-1} bands to assign γ-PVDF while 467 and 1275 cm^{-1} bands are used for beta phase determination. The 444 cm^{-1} band is also a beta-characteristic band; however, the gamma phase has an absorption band nearby, at 440 cm^{-1}. Therefore careful investigation must be made while determining the crystal phase using these peaks. In melt-crystallized samples, besides the existence of 811 cm^{-1} γ-band, an apparent increase is observed in the 1233 cm^{-1} band, especially at 0.05% OMS content and greater, as a result of OMS addition into PVDF.

Here, in PVDF/OMS nanocomposites melt-crystallized at high supercooling (150 °C), alpha phase formation is observed only up to 0.1% OMS, at which point gamma crystals substantially exist. We cannot rule out the possibility of a tiny amount of beta due to the observation of the band at 1275 cm^{-1}. This band may arise from beta formation after OMS addition. But it is also possible that the gamma phase chain contains some defects in its TTTGTTTG′ conformation. If imperfect gamma crystals induce more trans conformations (e.g., TTT or longer trans sequences) in addition to the gauche conformation, this may also contribute to the absorption at 1275 cm^{-1}, as well as to other frequencies representing beta absorption. For clarity, Table 1 shows major characteristic bands of the three different crystal phases from 400 to 1500 cm^{-1}. Also, Fig. 5 is supplied as a reference to differentiate alpha, beta, and gamma phases in their vibrational spectra. Three sample spectra were chosen dominant in each phase: 1. For α-phase, we show quenched neat PVDF; 2. For β-phase, we show PVDF with 4% OMS, cold-crystallized at 145 °C after quenching; and, 3. For γ-dominant sample, a 150 °C melt-crystallized PVDF/OMS nanocomposite with 1.0% OMS. Although we cannot rule out a tiny amount of beta TTT sequences in the gamma reference sample, a clear difference in the decisive bands can be seen between the beta and gamma dominant samples. FTIR data are consistent with X-ray data, confirming that melt-crystallization of nanocomposites of PVDF/OMS under "high" supercooling induces gamma phase formation, which is likely due to ion–dipole interaction in the molten state [21].

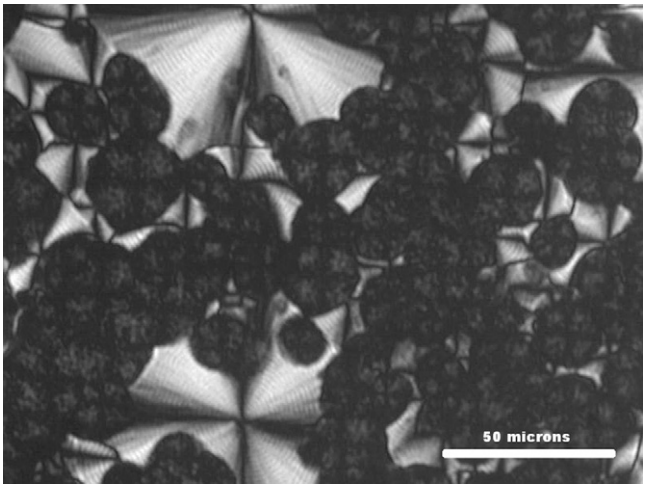

Fig. 7. Polarizing optical microscopy (A ⊥ P) image of nanocomposite sample of PVDF with 0.07% OMS, melt-crystallized 150 °C for 1 h. Numerous weakly birefringent gamma spherulites can be seen along with highly birefringent larger alpha spherulites appearing underneath.

3.3. Morphology

Fig. 6a–c shows the POM images of PVDF/OMS nanocomposites, 0, 0.032, and 0.07 wt% OMS, respectively, crystallized at 150 °C for 1 h from the melt. Only one type of spherulite was seen in the neat PVDF (Fig. 6a). These large, strongly birefringent spherulites comprise alpha phase crystals [9]. At higher magnifications (as an example, see the bright spherulites in Fig. 7), the typical banding

Table 2
Spherulite growth rate and average final diameter for melt-crystallized PVDF/OMS nanocomposites.#

OMS%	Growth rate[a] (μm/s, ±0.03)		Average diameter[b] (μm, ±0.8)	
	Alpha	Gamma	Alpha	Gamma
0.0	0.26	na	80	na
0.01	0.26	—	56	na
0.032	0.24	0.10	40	13
0.05	0.26	0.09	33*	15
0.07	0.26	0.13	33*	16*
0.10	0.24	—	25*	10*
0.32	0.19	—	24**	40**
1.00	—	—	—	—

All samples were melt-crystallized at 150 °C for 1 h.
na No dark spherulites were seen in these samples.
— Spherulites were too small for diameter to be determined.
* The areas with very irregular spherulites could not be counted.
** The area distribution was highly different in some regions. This number is the mean of the averages of two different size-distributed regions.
[a] Determined from the slope of spherulite diameter vs. time.
[b] Final diameter after completion of crystallization.

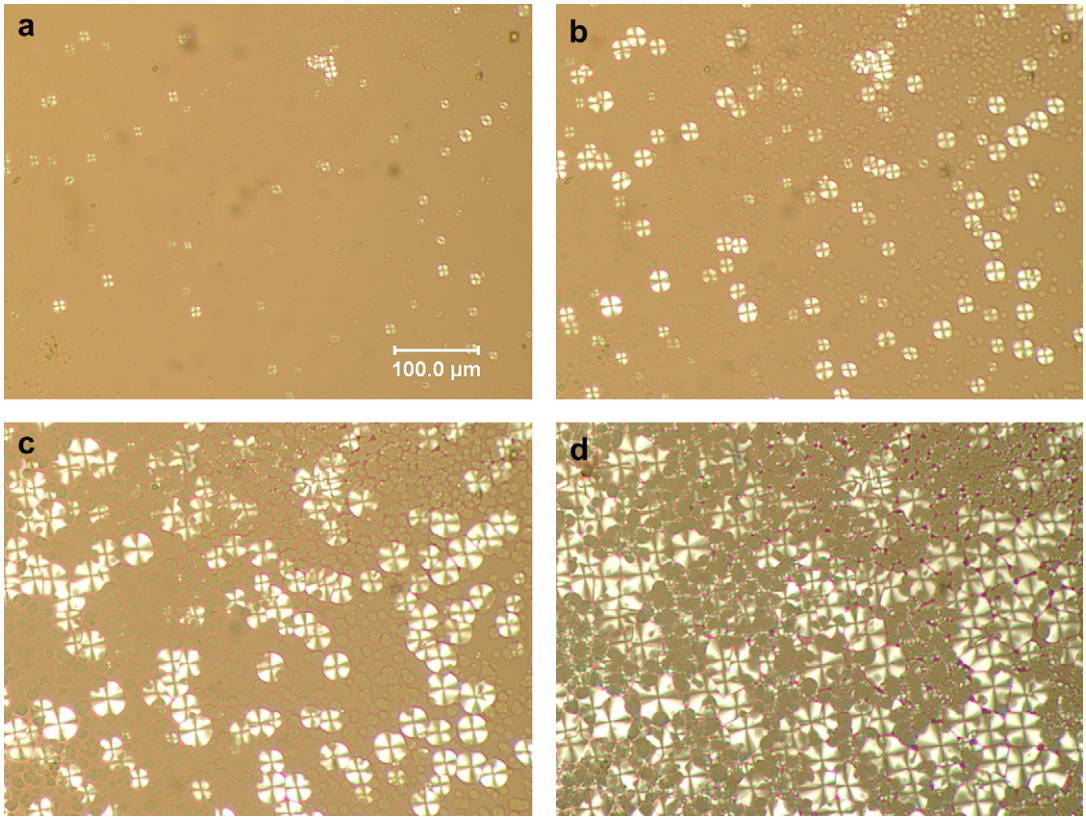

Fig. 8. (a–d) POM Images (A ⊥ P) of PVDF/OMS nanocomposite sample containing 0.07% OMS taken during melt-crystallization at 150 °C, at times: (a) 43 s, (b) 85 s, (c) 145 s, and (d) 235 s. Representative scale bar applies to all images.

pattern of concentric rings from twisting lamellae can be seen. The average spherulite diameter is about 80 μm for neat PVDF, and spherulites fill the entire viewing field. With addition of clay, darker, less birefringent spherulites of gamma phase appear (see Fig. 6b and c and an enlarged view in Fig. 7) in addition to the bright, highly birefringent spherulites of the alpha phase [8,9,33]. As seen in Fig. 7, these spherulites show a definite Maltese cross pattern of birefringence. Low-birefringence is known to occur as a result of extensive misorientation of lamellae with respect to the radii of gamma spherulites [11]. No banding is observed in these spherulites.

As the composition of OMS increases, from 0.01 to 0.07 wt% the diameters of the alpha spherulites decrease while the diameters of the gamma spherulites increase (see Table 2). When the OMS content exceeds 0.07 wt%, the diameters of both the alpha spherulites and gamma spherulites decrease. This originates from the effect of clay particles on nucleation of crystals. When the OMS composition exceeds 0.07 wt%, the nucleation density increases so

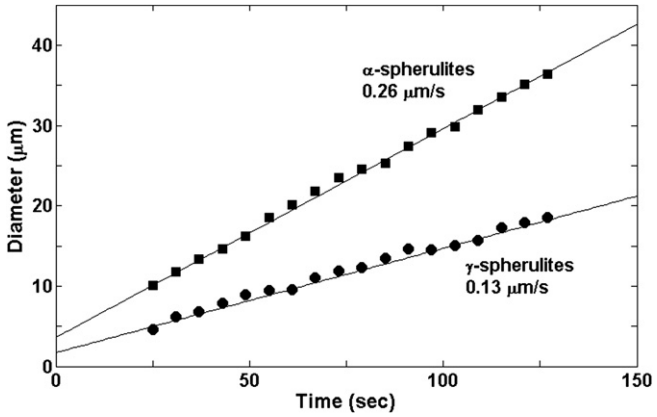

Fig. 9. Spherulite diameter vs. time during melt-crystallization at 150 °C for highly birefringent alpha spherulites (squares), and gamma spherulites (circles) seen in PVDF nanocomposites with 0.07% OMS. The diameters of three spherulites of each type were tracked for each time and the averages are plotted. Error bars are contained within the symbol. The slopes of the lines of the best fit are indicated.

Table 3
Melting temperatures of PVDF/OMS nanocomposite spherulites observed in POM, and in bulk films studied by DSC and WAXS.[#]

OMS%	α Spherulites[a]		γ Spherulites[b]	Bulk film[c]	Bulk film[d]
	T_m^{start} (°C) (±0.5)	T_m^{final} (°C) (±0.3)	T_m^{final} (°C) (±0.3)	T_m^{final} (°C) (±0.3)	T_m^{final} (°C) (±0.3)
0	168	171.5	None[e]	175	172
0.010	169	172	—	177	173
0.032	168	172	179	177	na
0.050	166	172	178	178	na
0.070	168	172	178	178	na
0.10	167	172	179	179	179
0.32	167	170	175	179	na
1.00	—	—	—	179	179

All samples were melt-crystallized at 150 °C for 1 h.
na Real-time WAXS was not applied to these samples.
— Unable to be determined.
[a] Bright spherulites are highly birefringent, banded, and comprise alpha phase crystals.
[b] Gamma spherulites are less birefringent and unbanded.
[c] Melting temperature from DSC during heating at 10 °C/min.
[d] Melting temperature from WAXS during heating at 10 °C/min.
[e] No dark spherulites were seen in these samples.

that at the highest composition we studied, 1.0 wt% OMS, both types of spherulites are too small to be resolved optically. However, nanocomposites with 0.32 wt% OMS showed an irregularity among other samples with an average of 40 μm diameter for the gamma spherulites. We have not observed any anomaly for this sample with other techniques; therefore this might be due to very low nucleation density as a result of sample preparation conditions. In addition, the area of the sample covered by gamma spherulites systematically increases with increase of OMS.

Fig. 8a–d shows a time series of POM images taken during melt-crystallization of PVDF nanocomposite with 0.07% OMS. The average diameters of both types of spherulites were measured as a function of crystallization time, and an example is shown in Fig. 9. From the slope of diameter vs. time, the linear growth rate of the spherulites was determined. These data are presented in Table 2. The growth rates of alpha crystals ranged from 0.24 to 0.26 μm/s and were almost the same for all OMS compositions. The one outlier was the nanocomposite sample with 0.32% OMS, which had alpha spherulite growth rate of 0.19 μm/s. The literature reports for alpha phase growth rates range from 0.15 [9] to 0.25 μm/s [34], so our data are consistent with prior reports. The smaller gamma spherulites have lower overall growth rate compared to alpha spherulites, between 0.09 and 0.13 μm/s. These results also agree with literature on gamma crystal growth rates [9]. For nanocomposites with 0.01 wt% OMS, gamma spherulites are too small to follow their growth with time, and the same was true as well in samples containing 0.1 wt% OMS and greater.

Growth rate curves do not intersect at the point (0,0) in Fig. 9. A possible explanation could be a time lag between the onset of isothermal crystallization and of image recording. It may also arise from early nucleation of spherulites just before the temperature reaches 150 °C while the hot stage is stabilizing its temperature from cooling to isothermal holding. Also, the extension of growth rate of gamma spherulites intersects the time axis at an earlier time, indicating an earlier nucleation than alpha spherulites, which is a known fact for PVDF crystallized at moderately high temperatures [10].

Melting behavior of melt-crystallized nanocomposites was also investigated with POM using a 10 °C/min heating rate. Birefringence of alpha spherulites started to decrease at 166–168 °C and spherulites totally disappeared by 171–172 °C. Gamma phase spherulites have a melting temperature about 6–7 degrees greater than their alpha counterparts, as expected [9,33]. Due to weakness of their birefringence it is not possible to detect the beginning of melting, but by 178–179 °C they vanish completely. As an exception, gamma spherulites in 0.32% sample show a final melting temperature 4 °C lower than others. All detected melting temperatures from POM, along with the melting temperatures obtained from DSC and X-ray, are listed in Table 3. Here, T_m^{start} is the temperature where the spherulites started to lose their birefringence. T_m^{final} represents the temperature at which complete melting of crystals is observed. For POM, final melting temperature was recorded when appearance of spherulites vanishes completely. In DSC, it is the temperature point where the fusion peak ends. In WAXS, T_m^{final} is recorded when crystal peaks have vanished and only an amorphous halo is left.

Spectral data on two types of spherulites are shown in Fig. 10a and b taken by FTIR and Raman microscopy, respectively. The alpha characteristic bands are either weak or absent in the weakly birefringent gamma spherulites (Fig. 10a and b, bottom spectra). In the infrared spectra, strong bands of gamma phase are seen at 840, 880, and 1233 cm^{-1} and a weak band occurs at 1117 cm^{-1}. Since use of KBr disks can lead to gamma phase formation [35], we also tested Raman spectra of the spherulites since Raman spectroscopy allows us to use inert glass substrates. The Raman spectra in Fig. 10b also clearly show the difference between the two types of spherulites. Gamma phase reflections (top spectrum) are observed at the vibrational frequencies at 265, 434, 513, 811, 840, 883 and 1234 cm^{-1} while alpha phase reflections (bottom spectrum) occur at 287, 488, 613, 796, 875, 1200 and 1429 cm^{-1}. Band assignments are taken from the literature [29–31]. The 1275 cm^{-1} band is observed in gamma spherulites in both infrared and Raman spectra.

The FTIR microscopy spectrum of the gamma spherulites in transmission mode shows a mixture of alpha and gamma bands. This probably arises from the fact that gamma spherulites lay over the top of the alpha spherulites so that transmittance data reflects alpha phase bands together with gamma spherulites. We also observed this situation optically, as seen in Figs. 7 and 8, where gamma spherulites lay over the alpha spherulites. Due to the greater growth rate of the alpha spherulites, these continue to grow underneath the dark γ spherulites during isothermal crystallization. The overlay structure of spherulites was tested with the help of AFM. The height difference in the *z*-axis between the two spherulites is seen in the AFM height images (Fig. 11). Two alpha spherulites next to each other show the same height (lower plot) while the gamma spherulite is higher than its alpha neighbors

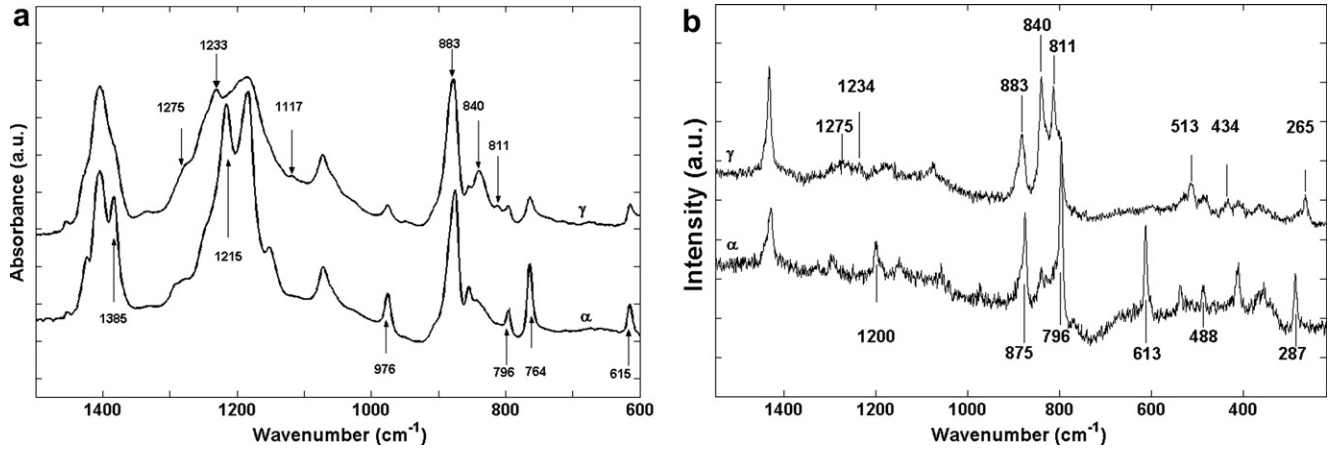

Fig. 10. (a and b) (a) FTIR microscopy absorbance spectra, and (b) Raman microscopy intensity spectra, of spherulites present in melt-crystallized PVDF/OMS composite sample with 0.05% OMS by weight. Spectra of less birefringent spherulites (marked as gamma) are shown in the upper curves; highly birefringent alpha spherulites are shown in the lower curves.

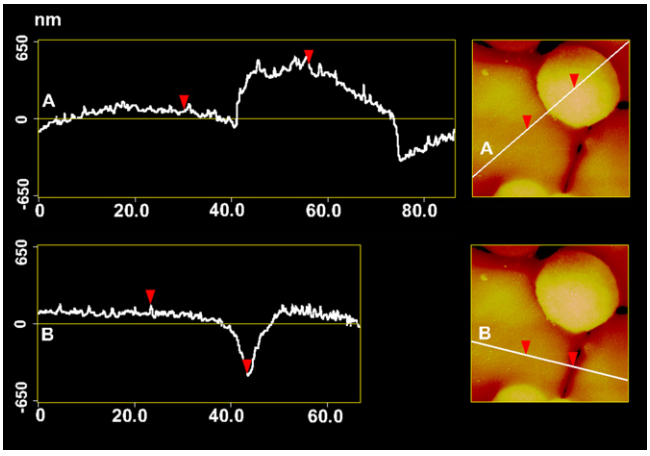

Fig. 11. AFM topographic images of PVDF/OMS nanocomposite film with 0.05% OMS by weight (right) with a scan size of 65 μm × 65 μm. Corresponding section analyses of the lines indicated by arrows are shown on the left for alpha and gamma spherulite neighbors (upper), and for two alpha spherulite neighbors (lower).

(upper plot). This phenomenon has been observed before in polymer nanocomposites with organic layered silicates and explained by surface free energy effects [36]. The clay migrates to the sample surface in the molten state due to a difference in the interfacial tension between clay and polymer, and the surface free energy of the polymer. This also explains why no impingement occurs between alpha and gamma spherulites, which in homopolymer PVDF causes distorted shapes (like teardrops) in gamma spherulites when they are next to alpha counterparts, due to their different growth rate [9,32]. Here, the gamma spherulites grow freely over the top of the alpha phase spherulites forming spherical shapes.

3.4. Thermal behavior

Fig. 12 shows the DSC stacked plots of nanocomposites during heating at 10 °C/min. Neat PVDF (bottom curve) has two endothermic peaks at 156 °C and 169 °C. The major peak at 169 °C is due to the alpha crystals melting. The lower endotherm is attributed to the less perfect crystals formed during the cooling after melt-crystallization at 150 °C. The lower temperature melting peak is not observed in nanocomposites with OMS content greater than 0.05 wt%. The higher melting temperature peak has been mistakenly attributed to beta crystal melting in some PVDF nanocomposite work due to literature reference confusion. Prest and Luca, in 1975, found a new spherulite type having different morphology from alpha crystal spherulites and they defined the new resulting phase as "beta" since the gamma phase structure was still under investigation and was not known well at that time [6,32]. In their work, Prest and Luca determined "beta" phase T_m (which later was found actually to be *gamma*) at a temperature 6–7 °C higher than alpha. Although this was corrected in following papers [9], it has been cited in the literature many times, even in a review article [37], and this confusion continues up to the present date in the literature. Coincidentally, in the first PVDF nanocomposite work by Priya and Jog [38,39], melting points of PVDF with clay added shifted to higher temperature, agreeing with this mistaken literature. In their work, observation of beta phase was correctly confirmed by other techniques beside DSC, but quite a number of subsequent nanocomposite works [1,12–14,16,40] thereafter cited Priya and Jog [38,39] for the beta melting point. When X-ray and FTIR data interpretations are carefully conducted, this does not result in any confusion. However, along with misinterpretation of melting point data, lack of clarity in differentiating WAXS peaks for different phases, and the similarity of vibrational spectra of beta and gamma phases, this confusion could lead to incorrect or inadequate assessment of the phases [16,20,40,41].

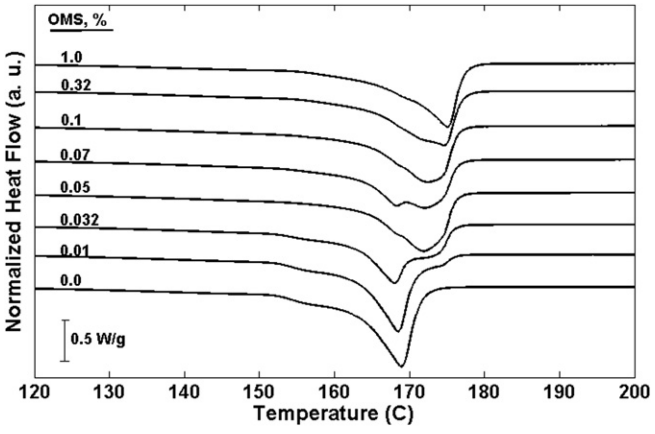

Fig. 12. DSC heating curves of melt-crystallized PVDF/OMS samples at 150 °C, with OMS percentages indicated on the figure. Heating rate is 10 °C/min.

Comparing the results of WAXS, FTIR and POM, we conclude that the higher melting point around 174 °C, which shows up first in nanocomposites with 0.01 wt% OMS, is a gamma crystal melting. Alpha and gamma crystal melting peaks co-exist from 0.01 wt% OMS up to 0.07 wt% OMS. For larger OMS content, the alpha crystal endotherm weakens significantly, and the alpha crystal endotherm remains only as a shoulder on the gamma crystal endotherm.

Table 4 shows melting peak temperatures of each endotherm for all samples and associated endotherm area and degree of crystallinity. Addition of OMS results in a small increase (~1 °C) in gamma crystal melting point. We did not observe any significant change in the alpha endotherm, or in the lower temperature endotherm. The disappearance of the lower melting endotherm for OMS content above 0.05 wt% shows the role OMS plays as a nucleating agent. This nucleation effect is also observed on subsequent non-isothermal cooling of nanocomposites at 10 °C/min, as an increase in crystallization temperature, T_c. We found that T_c increases by about 10 °C, from 135.1 °C for neat PVDF to 144.8 °C for 1.0 wt% OMS.

Crystallinity was calculated from melting endotherm area ratio to the heat of fusion of 100% crystalline PVDF, 104.6 J/g [23].

Table 4
Melting and crystallization temperature, heat of fusion, and crystallinity index obtained from DSC and WAXS for nanocomposites of PVDF with Lucentite STN.#

OMS (%)	T_m[a] (°C, ±0.3)			T_c[b] (°C, ±0.3)	ΔH_f[c] (J/g, ±2.0)	ϕ_c[d] (±0.02)	f_c[e] (±0.05)
0	156.2	168.9	None[f]	135.1	50	0.48	0.50
0.010	156.2	168.5	174.1	137.9	50	0.48	0.52
0.032	156.6	168.1	174.1	139.2	47	0.45	0.45
0.050	None[f]	168.1	174.2	138.6	48	0.45	0.38
0.070	None	168.3	174.3	138.9	49	0.46	0.34
0.10	None	168.5	174.7	141.6	47	0.44	0.36
0.32	None	168.5	174.8	142.9	48	0.45	0.34
1.00	None	169.1	175.2	144.8	48	0.45	0.35

All samples were initially melt-crystallized at 150 °C for 1 h.
[a] Determined from endotherm peak temperature during reheating at 10 °C/min.
[b] Determined from exotherm peak temperature during cooling from 200 °C at 10 °C/min.
[c] Determined from total endotherm area during heating at 10 °C/min.
[d] Crystallinity from DSC analysis of endotherm area using 104.6 J/g as the heat of fusion of PVDF [23].
[e] Crystallinity from WAXS analysis of (crystal peak area)/(total area).
[f] No peak of this type was seen in the DSC scan.

Crystallinity obtained from DSC is nearly constant for all OMS contents, but decreases from 0.50 to 0.35 when obtained from WAXS peak analysis. The difference in crystallinity acquired by DSC and WAXS analysis might be explained by considering that DSC accounts for melting of all crystals, no matter their level of perfection. But WAXS crystallinity index only refers to those crystals large enough to give good coherent scattering. Within the error bars on the crystallinity measurements, the two techniques show good agreement at low OMS content.

4. Conclusions

Nanocomposites of poly(vinylidene fluoride) with organically modified silicates have been investigated at low compositions after melt-crystallization under "high" supercooling. We observed that OMS addition results in gamma phase formation in PVDF melt-crystallized samples, whereas OMS addition resulted in beta phase previously [1] in cold-crystallized samples.

X-ray and FTIR analyses showed the gamma reflections increase with an increase in OMS content in PVDF. When OMS exceeds 0.1 wt%, alpha phase crystals were substantially diminished or did not exist. Crystallinity index was affected by OMS addition, showing a decrease from 0.50 to 0.35. WAXS and FTIR analysis showed only a slight possibility of beta phase existing along with gamma crystals.

With the addition of OMS, weakly birefringent spherulites have been observed along with, but lying on top of, strongly birefringent alpha spherulites. The FTIR and Raman microscopy spectra of these two types of spherulites show that the less birefringent spherulites are in the gamma phase. Their size increases while OMS percentage increases up to 0.07% and the area covered by gamma spherulites increases with the addition of OMS. Gamma spherulites were observed to lie over their alpha counterparts, resulting in non-distorted spherical shapes.

DSC and WAXS real-time results indicate a shift in melting temperature of nanocomposites to higher temperatures with an increase in OMS. Over 0.05 wt% OMS, the gamma melting endotherm is dominant. Final melting temperatures observed in POM show good agreement with DSC results.

Finally, we addressed ambiguities arising in determining PVDF crystallographic phases, and we correct the phase identification errors which have persisted up to this point in the literature based on melting point confusion. Crystal phase identification for PVDF nanocomposites was discussed and clarified, based on X-ray scattering, vibrational spectra, and thermal analysis. For reference, we provide a vibrational band list, indicating the close, or overlapping bands, of the three phases of PVDF: α, β and γ.

Acknowledgements

The authors thank the National Science Foundation, Polymers Program of the Division of Materials Research, for support of this research through grants DMR-0406127. Undergraduate summer interns Alpern, Amare, Dolan, Jones and Washington performed the research reported herein, at Tufts University. A portion of the X-ray scattering work was conducted at the Brookhaven National Laboratory, National Synchrotron Light Source, Advanced Polymers Beamline X27C supported by the Department of Energy.

References

[1] Buckley J, Cebe P, Cherdack D, Crawford J, Ince BS, Jenkins M, et al. Polymer 2006;47:2411.
[2] Gunduz BS. "Impacts of Nanosilicates on Phase Structure and Transitions of Poly(vinylidene fluoride)", PhD dissertation, Tufts Univ.; 2009.
[3] Nakamura S, Sasaki T, Funamoto J, Matsuzaki K. Makromol Chem 1975;176:3471.
[4] Mancarella L, Martuscelli E. Polymer 1977;18:1240;
Kawai H. Jpn J Appl Phys 1969;8(7):1975.
[5] Welch GJ, Miller RL. J Polym Sci Polym Phys Ed 1976;14:1683.
[6] Prest Jr WM, Luca DJ. J Appl Phys 1975;46:4136.
[7] Lovinger AJ, Keith HD. Macromolecules 1979;12:919.
[8] Morra BS, Stein RS. J Polym Sci Polym Phys Ed 1982;20:2243.
[9] Lovinger AJ. J Polym Sci Polym Phys Ed 1980;18:793.
[10] Lovinger AJ. Polymer 1980;21:1317.
[11] Gregorio R, Capitao RC. J Mater Sci 2000;35:299.
[12] Pramoda KP, Mohamed A, Phang IY, Liu T. Polym Int 2005;54:226.
[13] Sadeghi F, Ajji A. Polymer 2008;44:7899.
[14] Causin V, Carraro ML, Marega C, Saini R, Campestrini S, Marigo A. J Appl Polym Sci 2008;109:2354.
[15] Priya L, Jog JP. J Polym Sci Part B Polym Phys 2003;89:2036.
[16] Ince-Gunduz BS, Amare D, Alpern R, Cebe P, Crawford J, Dolan B, et-al. In: Smart dielectric polymer properties, characterization and their devices, edited by Bharti V, Cheng Z, Zhang QM, Bar-Cohen Y, Sessler GM, (Mater. Res. Soc. Symp. Proc. 949E, Warrendale, PA, 2007), C03–05.
[17] Asai K, Okamoto M, Tashiro K. Polymer 2008;49:4298.
[18] Dillon DR, Tenneti KK, Li CY, Ko FK, Sics I, Hsiao BS. Polymer 2006;47:1678.
[19] Song D, Yang R, He L. J Mater Sci 2007;42:8408.
[20] Patro TU, Mhalgi MV, Khakhar DV, Misra A. Polymer 2008;49:3486.
[21] Ramasundaram S, Yoon S, Kim KJ, Park C. J Polym Sci Part B Polym Phys 2008;46:2173.
[22] Available from: http://www.cbc.co.jp/indexe_n.html.
[23] Nakagawa K, Ishida Y. J Polym Sci Part B Polym Phys 1973;11:2153.
[24] Bachmann M, Lando JB. Macromolecules 1981;14:40.
[25] Lando JB, Olf HG, Peterlin A. J Polym Sci Part A-1 1966;4:941.
[26] Lovinger AJ. Macromolecules 1981;14:322.
[27] Hasegawa R, Takahashi Y, Chatani Y, Tadokoro H. Polym J 1972;3:600.
[28] MATLAB™ The Mathworks. Natick, MA; 2000.
[29] Kobayashi M, Tashiro K, Tadokoro H. Macromolecules 1975;8:158;
Yang D, Chen Y. J Mater Sci Lett 1987;6:599.
[30] Bachmann MA, Gordon WL. J Appl Phys 1979;50:6106.
[31] Kressler J, Schafer R, Thomann R. Appl Spectrosc 1998;52:1269.
[32] Lovinger AJ. Poly(vinylidene fluoride). In: Bassett DC, editor. Developments in crystalline polymers-1. London: Applied Science Publishers; 1982.
[33] Gianotti G, Capizzi A, Zamboni V. Chim Ind 1973;55:501.
[34] Penning JP, St. John Manley R. Macromolecules 1996;29:84.
[35] Miyazaki T, Takeda Y, Akasaka M, Sakai M, Hoshiko A. Macromolecules 2008;41:2749.
[36] Lewin M. Fire Mater 2003;27:1. Lewin M, Mey-Marom A, Frank R. Polym Adv Tech 2005;16:429. Lewin M. Polym Adv Tech 2006;17:758.
[37] Gregorio R, Cesari M, Chaves N, Nociti PS, Mendonca JA, Lucas AA. The polymeric materials encyclopedia. Boca Raton, FL: CRC; 1996.
[38] Priya L, Jog JP. J Appl Polym Sci 2003;89:2036.
[39] Priya L, Jog JP. J Polym Sci Part B Polym Phys 2003;41:31.
[40] Wu T, Xie T, Yang G. J Polym Sci Part B Polym Phys 2009;47:903.
[41] Yu W, Zhao Z, Zheng W, Long B, Jiang Q, Li G, et al. Polym Eng Sci 2009;49:491.